

RESEARCH ARTICLE

[View Article Online](#)
[View Journal](#)


Cite this: DOI: 10.1039/d6qi00339g

Nickel(II) porphyrin/fullerene C₇₀ porous molecular cocrystal featuring a robust one-dimensional channel

 Nobuhiro Sato,^a Kosuke Toki,^a Tomoki Tateishi,^{id} ^{a,b} Masaya Tsumura,^c
 Ryojun Toyoda,^{id} ^a Shinya Takaishi,^{id} ^a Yuki Kurashige,^{id} ^c Kuniyoshi Sugimoto^{id} ^d
 and Ryota Sakamoto^{id} ^{*a,e}

Molecular cocrystals are crystalline materials composed of multiple types of molecular components held together by noncovalent interactions. Among these, porphyrin–fullerene cocrystals represent a well-studied class of supramolecular assemblies. The close packing arrangement between porphyrins and fullerenes is known to contribute to high crystallinity and structural stability. Porphyrin–fullerene cocrystal systems including C₆₀, which has a spherical shape, have provided insights on intermolecular interaction. In contrast, cocrystals incorporating C₇₀, which has an ellipsoidal shape, remain relatively unexplored, and the influence of fullerene shape on cocrystal structures and stability remains unclear. In this study, we investigate the differences between C₆₀ and C₇₀ using cocrystals of a nickel(II) porphyrin derivative (NiTEPP) with these fullerenes. Two distinct cocrystals were successfully obtained: the porous cocrystal NiTEPP/C₇₀ featuring one-dimensional channels, and the nonporous crystal NiTEPP/C₇₀-n. High-pressure single-crystal X-ray diffraction results show that these cocrystals maintained their single crystal structure under high pressure. Furthermore, intermolecular interaction energies depending on the fullerene species were evaluated using density functional theory calculations. The combined experimental and theoretical results demonstrate that the shape of the fullerene plays a crucial role in governing intermolecular interactions and structural stability, and these results provide valuable guidelines for the rational design of molecular cocrystals with controlled intermolecular interactions.

Received 19th February 2026,

Accepted 7th April 2026

DOI: 10.1039/d6qi00339g

rsc.li/frontiers-inorganic

Introduction

Molecular cocrystals formed by the self-assembly of multiple molecular components has attracted increasing attention in recent years.^{1–3} By precise controlling intermolecular interactions⁴ and molecular geometries,⁵ it is possible to enhance the molecular ordering⁶ and structural stability.⁷ Cocrystallization enables the realization of structures and packing motifs that are not accessible in conventional unimolecular crystals,^{8,9} thereby expanding the scope of crystal engineering based on the inherent flexibility and diversity of

molecules.^{10–12} Furthermore, studies on molecular cocrystals play a crucial role in understanding of intermolecular interactions^{13–15} The elucidation of the principles governing precise molecular arrangements is expected to facilitate the design of molecular assemblies and future applications in functional materials.^{16–19}

Among molecular cocrystals, porphyrin–fullerene systems have emerged as a well-studied class of supramolecular assemblies.^{20–22} In these cocrystals, porphyrin molecules are regularly arranged around fullerene molecules, and intermolecular interactions— π – π stacking interactions and van der Waals forces—are known to contribute significantly to stabilize the crystal structure.^{23–25} The close contact of fullerene molecules with the porphyrin planes^{26,27} results in characteristic molecular packing, thereby improving the crystallinity and stability of the cocrystals.²⁴ To date, numerous porphyrin–fullerene cocrystals based predominantly on spherical C₆₀ have been reported.^{27–31} These results provide important insights into the structural features and design principles of molecular crystals. In contrast, reports on molecular cocrystals incorporating ellipsoidal C₇₀ are relatively limited compared with those

^aDepartment of Chemistry, Graduate School of Science, Tohoku University, 6-3 Aramaki Aza-Aoba, Aoba-ku, Sendai 980-8578, Japan. E-mail: ryota.sakamoto.e3@tohoku.ac.jp

^bFrontier Research Institute for Interdisciplinary Sciences (FRIS), Tohoku University Aramaki aza Aoba 6-3, Aoba-ku, Sendai 980-8578, Japan

^cDepartment of Chemistry, Graduate School of Science, Kyoto University, Kitashirakawa Oiwake-cho, Sakyo-ku, Kyoto, Japan

^dDepartment of Chemistry, Kindai University, 3-4-1 Kowakae, Higashi-Osaka, Osaka 577-8502, Japan

^eDivision for the Establishment of Frontier Sciences of Organization for Advanced Studies at Tohoku University, 2-1-1 Katahira, Aoba-ku, Sendai 980-8577, Japan



involving C_{60} .^{32–34} Consequently, systematic investigations into the differences in intermolecular interactions between porphyrins and different fullerene species, such as C_{60} and C_{70} , as well as their impact on cocrystal structures and stability, remain scarce.³⁵ Correspondingly, cocrystal systems involving metalloporphyrin derivatives in which both C_{60} and C_{70} afford the same crystal system remain limited.^{36,37}

In this situation, we previously prepared a cocrystal composed of a Ni-porphyrin derivative **NiTEPP**^{38,39} (Fig. 1a) and C_{60} (hereafter **NiTEPP/C₆₀**).⁴⁰ The structure of **NiTEPP/C₆₀** was characterized and analyzed by single-crystal X-ray diffraction (scXRD) measurement. This measurement revealed that porphyrin molecules regularly encapsulate C_{60} , forming two-dimensional honeycomb networks, in which three porphyrin molecules surround a single C_{60} molecule. These honeycomb layers stack along the *c* axis in AA* stacking mode. Owing to the stacking manner of the layers and the molecular ordering, permanent one-dimensional channels were confirmed to exist

in the crystal lattice. These structural features lead to the formation of a crystal with the $P\bar{3}c1$ space group. The presence of the two-dimensional honeycomb structure with intrinsic voids, together with its remarkable stability under acidic and basic conditions as well as external pressure, is rare among molecular crystals and represents a highly unique structural feature.⁴¹ Furthermore, reversible adsorption and desorption behavior toward solvents and gases demonstrates the functional utility of the one-dimensional channel in the crystal.

In this study, we report the preparation of two types of cocrystals composed of **NiTEPP** and C_{70} . These structures were thoroughly characterized by scXRD measurements. One cocrystal, **NiTEPP/C₇₀**, is isostructural with **NiTEPP/C₆₀**. In **NiTEPP/C₇₀**, C_{70} molecules occupy both axial positions of Ni center in **NiTEPP**. The porphyrin-to-fullerene ratio is determined to be 3 : 2 in **NiTEPP/C₇₀**. The other one is **NiTEPP/C_{70-n}** which has no void. In **NiTEPP/C_{70-n}**, only one axial position is occupied by a **NiTEPP** molecule, leading to a different ratio of **NiTEPP**

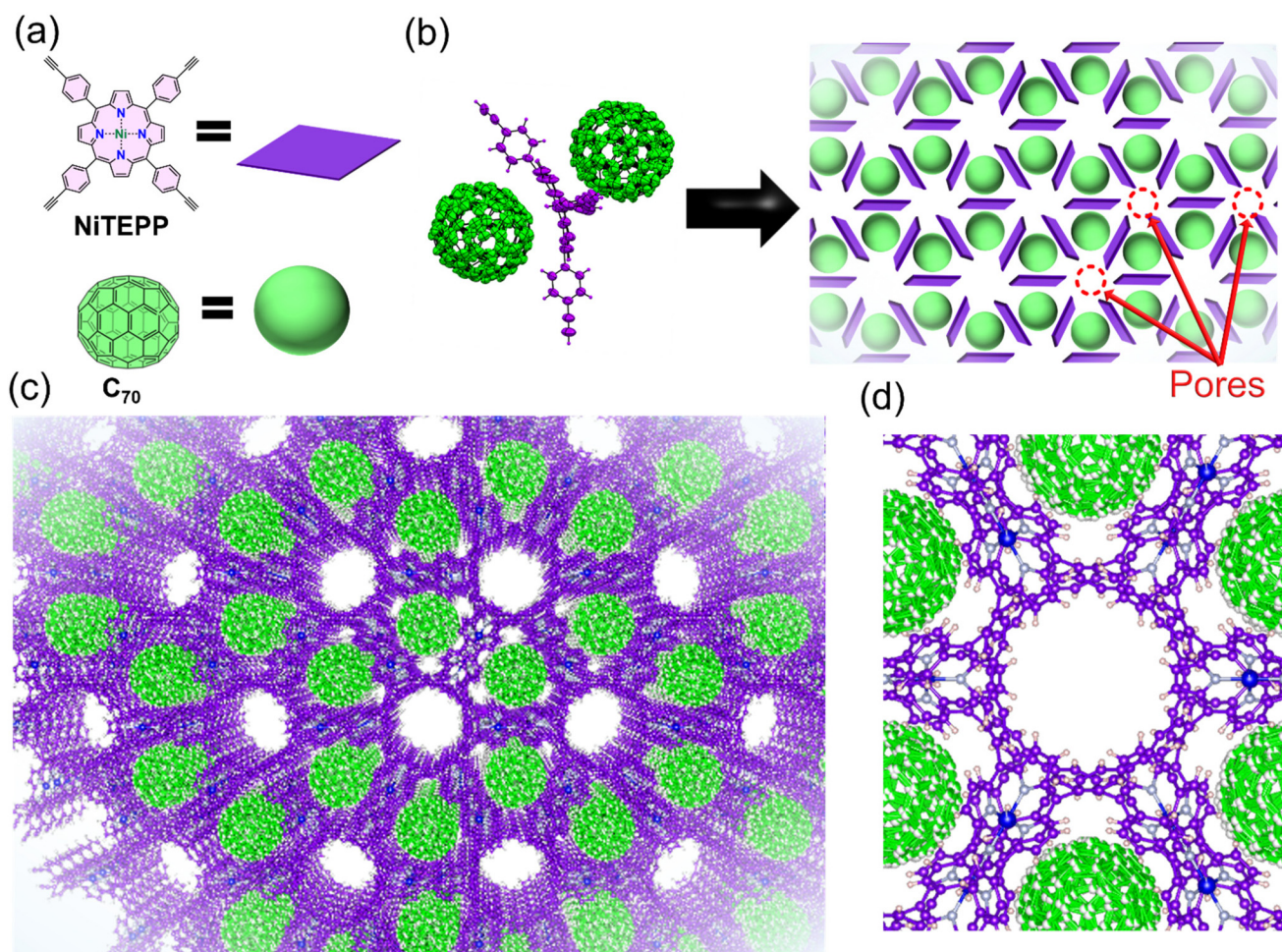


Fig. 1 Schematic illustration of the single-crystal structure of porous **NiTEPP/C₇₀** cocrystal. (a) Molecular structures of **NiTEPP** and C_{70} . **NiTEPP** and C_{70} are shown in purple and green, respectively. (b) Schematic illustration of the interaction between **NiTEPP** and C_{70} and the resulting honeycomb 2D network (measured at 120 K; thermal ellipsoids are drawn at the 50% probability level). (c) Stereoscopic crystal structure of **NiTEPP/C₇₀** viewed along the *c*-axis. (d) scXRD structure of **NiTEPP/C₇₀** viewed along the *c*-axis displaying Q peaks with intensities of more than 0.5 e^{-3} were set to be shown, while no significant residual electron density is observed in the channel.



and fullerene molecules, 1 : 1, in **NiTEPP/C₇₀-n**. DFT calculation revealed that **NiTEPP/C₇₀** exhibits a higher interaction energy than its **C₆₀** analogue, which is likely to be attributed to the elongated molecular shape of **C₇₀**. In contrast, **NiTEPP/C₇₀-n** shows a lower interaction energy compared to **NiTEPP/C₇₀**. These results demonstrate the effect of **C₇₀** incorporation instead of **C₆₀** on intermolecular interactions in the cocrystal with **NiTEPP**.

Results and discussion

NiTEPP was synthesized according to the previously reported procedure, and cocrystallization of **NiTEPP** with **C₇₀** was attempted using crystallization conditions analogous to those employed for **NiTEPP/C₆₀**.⁴⁰ However, the cocrystallization was unsuccessful using the liquid–liquid diffusion method. After optimization of the crystallization conditions, a vapor diffusion method (Fig. S1), using a 1 : 1 (v/v) mixture of **CHCl₃** and **CS₂** as the good solvent and hexane as the poor solvent, afforded black rod-shaped crystals of **NiTEPP/C₇₀** deposited on the inner wall of the vial.

The structure of **NiTEPP/C₇₀** was characterized by scXRD measurement (Fig. 1, S2 and Table S1). Unlike the previously reported **NiTEPP/C₆₀** cocrystal, **C₇₀** molecule does not possess a threefold rotational symmetry. The assignment of **C₇₀** molecules in **NiTEPP/C₇₀** required a disorder treatment that a single **C₇₀** molecule was modelled over three symmetry equivalent orientations because the $P\bar{3}c1$ possesses a threefold rotational axis throughout the crystal (Fig. S3). The crystal system of **NiTEPP/C₇₀** is formed by the arrangement of **C₇₀** molecules along both axial positions of **NiTEPP**, similar to **NiTEPP/C₆₀** (Fig. 1b). The interactions of three **NiTEPP** molecules surrounding a single **C₇₀** molecule give rise to a two-dimensional honeycomb network with a porphyrin-to-fullerene ratio of 3 : 2, extending along the *a* and *b* axes. This two-dimensional honeycomb network is stacked along the *c* axis in an eclipsed stacking mode, leading to the formation of one-dimensional channels running parallel to the *c* axis belonging to the space group $P\bar{3}c1$ with permanent voids (Fig. 1c). For the system of **NiTEPP/C₆₀**, when the residual electron density (Q-peak) within the channels was below $0.5 \text{ e } \text{Å}^{-3}$, simultaneous thermogravimetry-mass spectrometry measurements indicated that no solvent molecules were present in the voids. For **NiTEPP/C₇₀**, no Q-peaks greater than $0.5 \text{ e } \text{Å}^{-3}$ were found in the channel. This result suggests that no solvent molecules are present in the voids. At 120 K, the unit-cell parameters of **NiTEPP/C₇₀** were determined to be $a = 23.05$ and $c = 21.90$ Å (Table S1). Compared with those of **NiTEPP/C₆₀** ($a = 22.13$ and $c = 21.66$ Å), these values correspond to expansions of 1.97% along the *a* axis and 2.85% along the *c* axis, respectively. The unit-cell volume of **NiTEPP/C₇₀**, $10\,080 \text{ Å}^3$, corresponds to the expansion of 6.93% from **NiTEPP/C₆₀** (9188 Å^3). In previously reported cocrystals of metalloporphyrin with **C₆₀** and **C₇₀** that afford same crystal system, the unit cell volumes change negligibly (within 1%).^{36,37} In contrast, the present system rep-

resents a unique cocrystal in which the same crystal system is retained for both **C₆₀** and **C₇₀**, while exhibiting a pronounced change in unit cell volume of 6.9%. To evaluate the geometric relationship among fullerene molecules in detail, the angles and distances of the component molecules were analysed. All disorder-modelled **C₇₀** molecules, the long molecular axis is found to be tilted by 34.7° relative to the *c* axis (Fig. S4). In the case of the shortest centroid–centroid distances between fullerenes, **NiTEPP/C₆₀** shows the distances of 13.29 Å along the two-dimensional network direction (Fig. S5a) and 10.85 Å along the *c* axis (Fig. S5b), respectively. In **NiTEPP/C₇₀**, the distances increase to 13.71 (Fig. S5c) and 11.15 Å (Fig. S5d), respectively. In addition, the distances between the Ni center of **NiTEPP** and the centroid of the fullerene molecule was evaluated in both **NiTEPP/C₆₀** and **NiTEPP/C₇₀**. At 120 K, the distances are determined to be 7.05 Å for **NiTEPP/C₆₀** and 7.19 Å for **NiTEPP/C₇₀**, respectively. Furthermore, based on a previous study,⁴² the angle of Ni center of **NiTEPP** and two mutually opposing *meso*-carbon atoms in the porphyrin, defined as α , are also determined to be 161.4° for **NiTEPP/C₆₀** and 159.5° for **NiTEPP/C₇₀**, respectively. The anisotropic, elongated geometry of **C₇₀** hinders the Ni(II)porphyrin from adopting a fully surrounding configuration, in contrast to spherical **C₆₀**. The geometric differences in the crystal are attributed to the nonspherical shape of the **C₇₀** molecule, which possesses an intrinsic long axis and is larger than **C₆₀**.

Next, the void volume was evaluated using the void calculation function implemented in Mercury. A probe radius of 1.8 Å was applied, following the same conditions as those used for **NiTEPP/C₆₀**. At 120 K, the void volume of **NiTEPP/C₆₀** was determined to be 1190 Å^3 per unit-cell, whereas that of **NiTEPP/C₇₀** was 1260 Å^3 . This value corresponds to an increase of 8.6% in **NiTEPP/C₇₀**. The calculated void fractions are 12.7% for **NiTEPP/C₆₀** (Fig. S6) and 12.9% for **NiTEPP/C₇₀** (Fig. S7). Furthermore, pore radius analysis (Fig. S8 and S9) revealed that the minimum pore radius was 3.34 Å for **NiTEPP/C₆₀** and 3.71 Å for **NiTEPP/C₇₀**, respectively. These observations suggest that the fullerene geometry modulates both the void fraction and pore size in the isostructural crystal structure.

We note that for **NiTEPP/C₇₀**, scXRD analysis was successfully performed even at ambient temperature (293 K; Fig. S10 and Table S2). The molecular arrangement of **NiTEPP** and **C₇₀** was determined to be same as the crystal structure of **NiTEPP/C₇₀** measured at 120 K. Compared with **C₆₀**, **C₇₀** possesses lower molecular symmetry and is more susceptible to orientational disorder, which generally makes scXRD analysis challenging.^{43,44} Consequently, only a limited number of crystal structures containing **C₇₀** have been successfully analyzed at ambient temperatures.^{22,45} For **NiTEPP/C₇₀**, although an increase in the degree of disorder of the **C₇₀** molecules was observed at 293 K, the crystals satisfied the standard crystallographic quality criteria when the same disorder model as that applied at 120 K was applied. The successful single-crystal structure determination at ambient temperature is attributed to the fact that the orientation of the **C₇₀** molecules is partially restricted by interactions with the porphyrin planes,⁴⁶ and



further constrained by the three-directional encapsulation of the C_{70} molecules by NiTEPP, which spatially confines the molecular position in the crystal lattice.

Furthermore, in the course of the recrystallization of NiTEPP and C_{70} , other single crystals with a morphology different from that of NiTEPP/ C_{70} were found, which were subjected to scXRD (referred to NiTEPP/ C_{70-n} ; Fig. 2, S11 and Table S3). Structural analysis for NiTEPP/ C_{70-n} revealed that the porphyrin and C_{70} molecules are closely arranged and that C_{70} is located on only one side of the NiTEPP axial position, unlike NiTEPP/ C_{70} . An adjacent porphyrin molecule occupies the opposite side of the porphyrin axial position. As a result, NiTEPP and C_{70} form a 1:1 complex, and dense packing of this complex within the crystal leads to the formation of a nonporous structure (Fig. 2). The asymmetric arrangement and nonporous structure of NiTEPP/ C_{70-n} contrasts with that of NiTEPP/ C_{70} . The distance between the Ni center of NiTEPP and the centroid of C_{70} molecule was evaluated in the same manner as for NiTEPP/ C_{70} . In NiTEPP/ C_{70-n} , this distance was determined to be 6.49 Å, which is quite shorter than those observed in the structures of NiTEPP/ C_{60} and NiTEPP/ C_{70} . The shortest Ni–C distance between NiTEPP and C_{70} was determined to be 2.87 Å, which is shorter than typical π - π stacking distances.²² This suggests that specific porphyrin–fullerene interactions contribute to the proximity between the two com-

ponents. In addition, the angle α of NiTEPP in NiTEPP/ C_{70-n} was measured using the same definition as mentioned above. Although two angles α can be defined for NiTEPP/ C_{70-n} due to the inequivalence of the front and back sides of the porphyrin plane, the smaller value was adopted as a representative descriptor of the structural distortion. As a result, α was determined to be 175.9°, which is markedly larger than those of NiTEPP/ C_{60} and NiTEPP/ C_{70} . This indicates that NiTEPP in NiTEPP/ C_{70-n} undergoes minimal curvature (Fig. 2a). In contrast to NiTEPP/ C_{70} , NiTEPP/ C_{70-n} adopts an asymmetric and densely packed 1:1 architecture in which C_{70} is positioned on only one side of NiTEPP. The different spatial arrangement in NiTEPP/ C_{70-n} leads to a nonporous structure with close intermolecular contact, even with the porphyrin–fullerene interactions stabilizing both the crystal structures of NiTEPP/ C_{70} and NiTEPP/ C_{70-n} .

Subsequently, the obtained crystals were subjected to a series of characterizations. Powder X-ray diffraction (PXRD) analysis (Fig. S12) revealed that the sample prepared *via* Fig. S1 contains NiTEPP/ C_{70} and NiTEPP/ C_{70-n} phases but is overall a multiphase mixture. Accordingly, all subsequent measurements were conducted using this mixture. To probe the solid-state interactions, spectroscopic analyses were performed. The IR spectrum (Fig. S13) exhibits characteristic bands attributable to both NiTEPP and C_{70} , confirming the

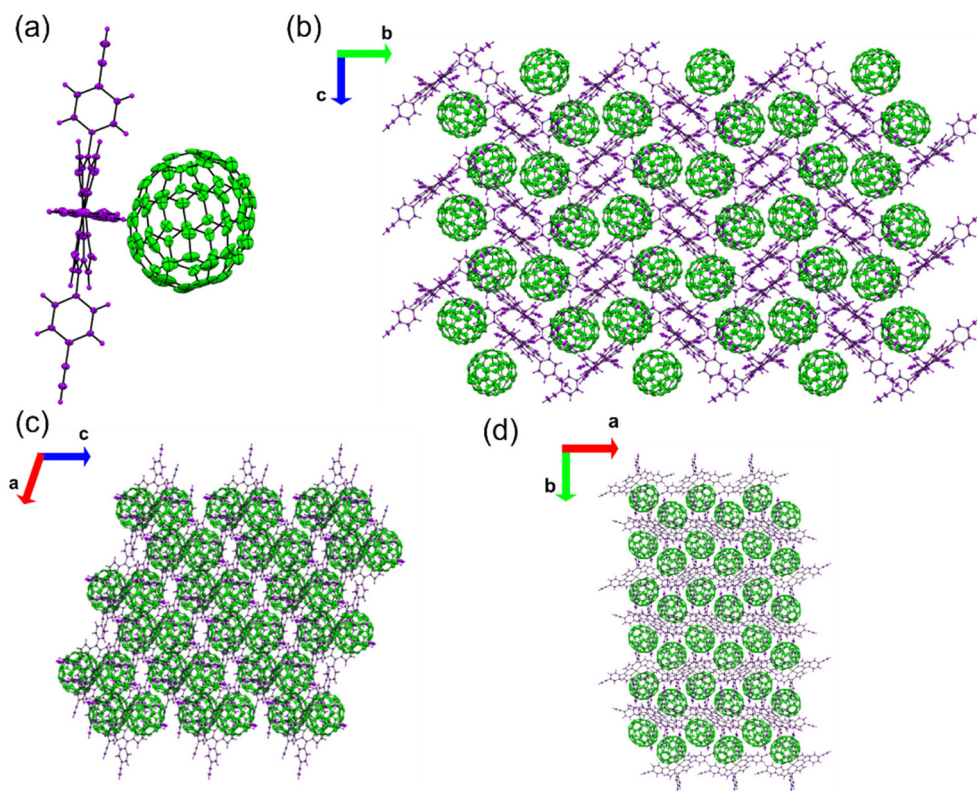


Fig. 2 Schematic illustration of the single-crystal structure of nonporous NiTEPP/ C_{70-n} cocrystal. (a) ORTEP drawing of NiTEPP/ C_{70-n} , showing that the Ni(II)porphyrin plane does not bend along with C_{70} . (b) Crystal packing structure of NiTEPP/ C_{70-n} viewed along a axis. (c) Crystal packing structure of NiTEPP/ C_{70-n} viewed along b axis. (d) Crystal packing structure of NiTEPP/ C_{70-n} viewed along c axis.



coexistence of these components. The solid-state UV-vis spectrum (Fig. S14) shows a distinct shift in the bands assignable to NiTEPP, which is attributed to intermolecular interactions with C₇₀ in the solid state. The direction of this shift is consistent with that observed in the previously reported NiTEPP/C₆₀ system,⁴⁰ supporting a similar interaction mode. N₂ gas sorption measurements at 77 K were then carried out using the mixture sample. The sorption isotherm (Fig. S15) exhibits Type I behavior, indicative of microporosity, and shows reversible adsorption-desorption, demonstrating stable uptake and release of N₂. From this N₂ sorption isotherm, a monolayer adsorption capacity (V_m) and Brunauer-Emmett-Teller (BET) surface area were estimated to be 49.2 cm³(STP) g⁻¹ and 214 m² g⁻¹, respectively. For comparison, theoretical values derived from the crystal structure are 60.9 cm³(STP) g⁻¹ and 265 m² g⁻¹, respectively. The smaller experimental values are attributed to the existence of nonporous NiTEPP/C_{70-n} crystals in the used solid sample, besides porous NiTEPP/C₇₀ crystals, which reduces the overall adsorption capacity. The pore size distribution was further evaluated from the adsorption isotherm using the NLDFT-GCMC method (Fig. S16). The distribution exhibits a maximum at 0.847 nm, slightly larger compared to that of NiTEPP/C₆₀, and indicates a slight increase in pore size consistent with the expansion of the unit cell.

Next, DFT calculations were performed using the CP2K program⁴⁷ to evaluate the interactions between the NiTEPP framework and fullerene molecules. A dispersion correction was applied to account for van der Waals interactions (see SI for the computational details). The structures of NiTEPP/C₆₀, three types of disordered NiTEPP/C₇₀, and NiTEPP/C_{70-n} were geometrically optimized. The interaction energies were then calculated as the difference between the energies of the total energy of the optimized cocrystal and the sum of the isolated NiTEPP framework and a single fullerene molecule. The interaction energies ΔE per fullerene molecule were calculated for these five optimized structures (Table 1). The interaction energy can be decomposed into four energetic components.⁴⁸ To clarify the nature of ΔE , we also evaluated the dispersion contribution ΔE_{disp} separately. Notably, the dispersion contribution accounts for most of the total interaction energy in all systems. Among the examined systems, NiTEPP/C₇₀ exhibits significantly larger stabilization ($\Delta E = 101.76$ kcal mol⁻¹, averaged over three symmetry related configurations) than NiTEPP/C₆₀ ($\Delta E = 94.98$ kcal mol⁻¹). This difference reflects the larger contact surface area between C₇₀ and NiTEPP framework. Importantly, the magnitude of ΔE in these systems is consider-

ably larger than values reported for conventional theoretical studies of supramolecular assemblies.^{48,49} This result suggests that the three-directional encapsulation by NiTEPP effectively amplifies the stabilization based on the dispersion contribution through simultaneous multipoint interactions. The stronger stabilization of C₇₀ relative to C₆₀ is consistent with previous theoretical studies.^{49,50} Conversely, NiTEPP/C_{70-n} exhibits a smaller interaction energy ($\Delta E = 88.47$ kcal mol⁻¹) compared with the three-directionally surrounded NiTEPP/C₇₀ cocrystal. Nevertheless, the magnitude of ΔE remains substantially large, even though in NiTEPP/C_{70-n} each C₇₀ interacts with only a single NiTEPP unit. This significant stabilization can be attributed to the proximity between NiTEPP and C₇₀ in NiTEPP/C_{70-n}, which enhances short-range dispersion interactions. The smaller overall interaction energy arises from the reduced number of NiTEPP units directly interacting with the C₇₀ molecule. Consequently, the overall contact surface area is reduced in NiTEPP/C_{70-n}, leading to fewer dispersion interactions per fullerene molecule. Overall, these results indicate that dispersion interactions dominate the stabilization of the NiTEPP/fullerene cocrystal structures and the strength of stabilization is determined by both the number of interacting NiTEPP units and their spatial arrangement around the fullerene molecules.

Finally, we investigated the pressure resistance of NiTEPP/C₇₀ and NiTEPP/C_{70-n} in their single-crystalline states. High-pressure scXRD measurements were conducted following the same procedure previously reported for NiTEPP/C₆₀.³⁸ Single-crystalline samples were placed in a diamond anvil cell, and scXRD measurements were performed at 300 K with gradually increasing pressure in the anvil cell. Under the low pressure at 0.60 GPa, NiTEPP/C₇₀ retained a quasi-trigonal crystal structure, and the unit-cell volume decreased monotonically with increasing pressure (Fig. 3a-d and Table S4). With increased external pressure to 1.4 GPa, the indexing match rate of the observed diffraction peaks against the unit-cell dropped sharply (Fig. 3b). This behaviour indicates that the crystal structure of NiTEPP/C₇₀ collapses in this pressure range of 0.60 to 1.4 GPa. Notably, the collapse pressure is lower than that of NiTEPP/C₆₀, which retains its single crystal structure up to 2.2 GPa.⁴⁰ Still, the level of pressure resistance for NiTEPP/C₇₀ remains relatively high even when compared with other porous organic crystals.^{51,52} Analysis of the changes in the lattice parameters as a function of the applied pressure revealed that, similar to NiTEPP/C₆₀, structural collapse in NiTEPP/C₇₀ is accompanied by elongation along the *c* axis and an increase in the γ angle (Fig. 3c and d). This deformation mode is consistent with the structural response expected when pressure is applied from the obtuse γ side of the rhombic unit-cell. The lower collapse pressure of NiTEPP/C₇₀ is likely attributable to the anisotropic molecular shape of C₇₀. Although the overall crystal symmetry is described by space group *P* $\bar{3}c1$ in both NiTEPP/C₇₀ and NiTEPP/C₆₀, local structural analysis indicates that the C₇₀ molecules do not occupy crystallographically equivalent positions relative to the three surrounding NiTEPP units. Such microscopic structural distortions are

Table 1 Calculated interaction energies (ΔE) and dispersion contributions (ΔE_{disp}) per fullerene

	ΔE (kcal mol ⁻¹)	ΔE_{disp} (kcal mol ⁻¹)
NiTEPP/C ₆₀	-94.98	-102.60
NiTEPP/C ₇₀ (type 1)	-102.05	-111.78
NiTEPP/C ₇₀ (type 2)	-102.05	-111.35
NiTEPP/C ₇₀ (type 3)	-101.17	-112.06
NiTEPP/C _{70-n}	-88.47	-94.93



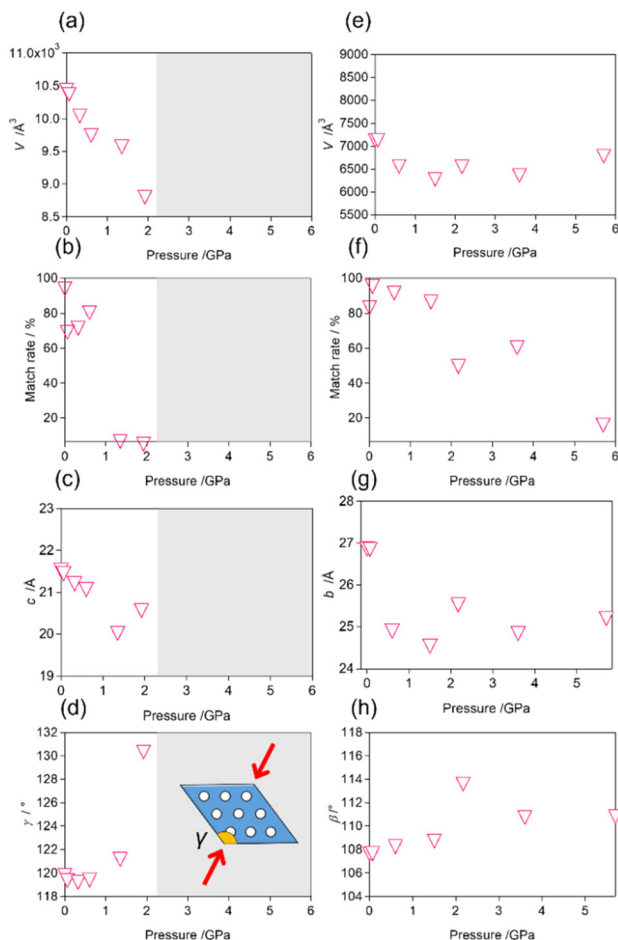


Fig. 3 (a–d) Changes in the cell parameters as a function of applied pressure for NiTEPP/C₇₀. (a) The unit cell volume V . (b) The match rate of detected diffraction peaks to the indexed unit cell. (c) The c axis length. (d) The γ angle. (e–h) Changes in the cell parameters as a function of applied pressure for NiTEPP/C_{70-n}. (e) The unit cell volume V . (f) The match rate of detected diffraction peaks to the indexed unit cell. (g) The b axis length. (h) The β angle. The ranges of both the vertical and horizontal axes are unified for NiTEPP/C₇₀ and NiTEPP/C_{70-n} for direct comparison. Note that pressures above 1.9 GPa were not measured for NiTEPP/C₇₀.

therefore considered to facilitate pressure-induced structural collapse.

In the case of NiTEPP/C_{70-n}, the unit-cell volume was slightly decreased with increasing pressure, compared to NiTEPP/C₇₀ (Table S5 and Fig. 3e). This difference in the decreased volume is likely because NiTEPP/C_{70-n} does not have any voids in its crystal structure. The limited compressible free volume is likely to be attributed for the smaller volume change against the applied pressure. When the pressure was increased from 3.6 to 5.7 GPa, the indexing match rate of the observed diffraction peaks against the unit-cell was significantly decreased (Fig. 3f), accompanied by an anomalous increase in the detected unit-cell volume. Unlike NiTEPP/C₇₀, neither the b axis length nor the β angle, both of which exhibited relatively large variations, exhibited a systema-

tic trend with increasing pressure (Fig. 3g and h). These results indicate that NiTEPP/C_{70-n} has a relatively high-pressure resistivity of among nonporous molecular crystals.⁵³

Conclusions

In this study, two types of the porphyrin-fullerene cocrystals were prepared from NiTEPP and C₇₀: porous NiTEPP/C₇₀ cocrystal and nonporous NiTEPP/C_{70-n} cocrystal. Single-crystal X-ray diffraction analyses of NiTEPP/C₇₀ and NiTEPP/C_{70-n} revealed the differences in the porphyrin-to-fullerene ratio and these packing arrangement. High-pressure scXRD measurements elucidated the pressure-dependent structural behaviors of both cocrystals and their structural robustness under high pressure. In addition, DFT calculations revealed that cocrystallization of NiTEPP with C₇₀ provides greater stabilization than that with C₆₀. The detailed comparison of the intermolecular interactions in NiTEPP/C₆₀ and NiTEPP/C₇₀ revealed that the increasing the contact surface area between C₇₀ and NiTEPP framework in NiTEPP/C₇₀ critically increased the porphyrin-fullerene interactions. The insights gained in this study provide valuable a useful guidance for the design of crystalline architecture based on intermolecular interactions and are expected to contribute to advances in crystal engineering and related fields.

Author contributions

N. S.: conceptualization, data curation, investigation, formal analysis, writing original manuscripts, review, and editing. K. T.: investigation. T. T.: writing original manuscripts, review, and editing. M. T.: calculation, writing computational section's manuscripts. R. T.: funding acquisition, methodology, resource, review, and editing. S. T.: methodology, resource. Y. K.: methodology on computational section, review, and editing. K. S.: high-pressure SXRD. R. S.: conceptualization, formal analysis, funding acquisition, methodology, project administration, resource, supervision, writing original manuscripts, review, and editing.

Conflicts of interest

There are no conflicts to declare.

Data availability

The data supporting this article have been included as part of the supplementary information (SI). Supplementary information: synthetic procedure, disorder process, X-ray crystallographic details, high pressure X-ray crystallographic details, and computational details. See DOI: <https://doi.org/10.1039/d6qi00339g>.



CCDC 2527177–2527179 contain the supplementary crystallographic data for this paper.^{54a–c}

Acknowledgements

This work was supported by JST-CREST (JPMJCR24S6 to R. S.) and JST-FOREST (JPMJFR203F to R. S. and JPMJFR221R to Y. K.). This work was also supported by MEXT/JSPS KAKENHI Grant Numbers (JP25H01644, JP25H01999, JP25H02031, JP24K01494, JP22H05145, JP25KJ0562). We acknowledge the Asahi Glass Foundation (R. S.) for financial support. The computation was partly performed at the Research Center for Computational Science, Okazaki, Japan (Project: 25-IMS-C029). A part of SXRD measurements was performed at SPring-8 BL02B1 with the approval of the Japan Synchrotron Radiation Research Institute (JASRI) (Proposal No. 2025B1724).

References

- 1 D. C. Sakhiya and C. H. Borkhataria, A review on advancement of cocrystallization approach and a brief on screening, formulation and characterization of the same, *Heliyon*, 2024, **10**, e29057.
- 2 J. Roshni and T. Karthick, A Comprehensive Review on Theoretical Screening Methods for Pharmaceutical Cocrystals, *J. Mol. Struct.*, 2025, **1321**, 139868.
- 3 S. Ren, G.-Y. Qiao and J.-R. Wu, Supramolecular-macrocycle-based functional organic cocrystals, *Chem. Soc. Rev.*, 2024, **53**, 10312–10334.
- 4 J. Alfuth, K. Kazimierzczuk, T. Połński and T. Olszewska, Intermolecular Hydrogen Bonding Directed by Aryl-Perfluoroaryl π - π Stacking Interactions, *Cryst. Growth Des.*, 2023, **23**, 6830–6839.
- 5 M. Donoshita, Y. Yoshida, M. Hayashi, R. Ikeda, S. Tanaka, Y. Yamamura, K. Saito, S. Kawaguchi, K. Sugimoto and H. Kitagawa, Various Stacking Patterns of Two-Dimensional Molecular Assemblies in Hydrogen-Bonded Cocrystals: Insight into Competitive Intermolecular Interactions and Control of Stacking Patterns, *Angew. Chem., Int. Ed.*, 2021, **60**, 22839–22848.
- 6 J. R. Palmer, S. B. Tyndall, G. C. Mantel, O. J. Buras, R. M. Young, M. D. Krzyaniak and M. R. Wasielewski, Molecular Cocrystal Packing Suppresses Hopping-Driven Decoherence of Excitonic Spin Qubits, *J. Am. Chem. Soc.*, 2025, **147**, 17394–17403.
- 7 L. Liu, J.-R. Wang and X. Mei, Enhancing the stability of active pharmaceutical ingredients by the cocrystal strategy, *CrystEngComm*, 2022, **24**, 2002–2022.
- 8 C. C. Seaton, Building Up Co-Crystals: Structural Motif Consistencies Across Families of Co-Crystals, *Proceedings*, 2020, **78**, 45.
- 9 C. Aakeröy, Is there any point in making co-crystals?, *Acta Crystallogr., Sect. B: Struct. Sci., Cryst. Eng. Mater.*, 2015, **71**, 387–391.
- 10 G. R. Krishna, R. Devarapalli, G. Lal and C. M. Reddy, Mechanically Flexible Organic Crystals Achieved by Introducing Weak Interactions in Structure: Supramolecular Shape Synthons, *J. Am. Chem. Soc.*, 2016, **138**, 13561–13567.
- 11 S. Hayashi, Elastic Organic Crystals of π -Conjugated Molecules: New Concept for Materials Chemistry, *Symmetry*, 2020, **12**, 2022.
- 12 P. Bombicz, T. Gruber, C. Fischer, E. Weber and A. Kálmán, Fine tuning of crystal architecture by intermolecular interactions: synthon engineering, *CrystEngComm*, 2014, **16**, 3646–3654.
- 13 G. Liu, S.-H. Wei and C. Zhang, Review of the Intermolecular Interactions in Energetic Molecular Cocrystals, *Cryst. Growth Des.*, 2020, **20**, 7065–7079.
- 14 A. J. Cruz-Cabeza, P. R. Spackman and A. V. Hall, The interplay between hydrogen bonds and stacking/T-type interactions in molecular cocrystals, *Commun. Chem.*, 2024, **7**, 284.
- 15 M. L. Clapham, R. R. Frontiera and C. J. Douglas, Mixed Rubrene Cocrystals Offer Insights into Intermolecular Interactions Influencing Crystal Packing, *Cryst. Growth Des.*, 2023, **23**, 3942–3946.
- 16 B. Li, L. Liu, Y. Wang, K. Liu, Z. Zheng, S. Sun, Y. Hu, L. Li and C. Li, Structurally diverse macrocycle co-crystals for solid-state luminescence modulation, *Nat. Commun.*, 2024, **15**, 2535.
- 17 W. Xu, G. Huang, Z. Yang, Z. Deng, C. Zhou, J.-A. Li, M.-D. Li, T. Hu, B. Z. Tang and D. L. Phillips, Nucleic-acid-base photofunctional cocrystal for information security and antimicrobial applications, *Nat. Commun.*, 2024, **15**, 2561.
- 18 L. Sun, Y. Wang, F. Yang, X. Zhang and W. Hu, Cocrystal Engineering: A Collaborative Strategy toward Functional Materials, *Adv. Mater.*, 2019, **31**, 1902328.
- 19 T. Wakahara, P. D'Angelo, K. Miyazawa, Y. Nemoto, O. Ito, N. Tanigaki, D. D. C. Bradley and T. D. Anthopoulos, Fullerene/Cobalt Porphyrin Hybrid Nanosheets with Ambipolar Charge Transporting Characteristics, *J. Am. Chem. Soc.*, 2012, **134**, 7204–7206.
- 20 P. Bhyrappa and K. Karunanithi, Porphyrin–Fullerene, C₆₀, Cocrystallates: Influence of C₆₀ on the Porphyrin Ring Conformation, *Inorg. Chem.*, 2010, **49**, 8389–8400.
- 21 Y. Hao, Y. Wang, L. Spree and F. Liu, Rotation of fullerene molecules in the crystal lattice of fullerene/porphyrin: C₆₀ and Sc₃N@C₈₀, *Inorg. Chem. Front.*, 2021, **8**, 122–126.
- 22 P. D. W. Boyd, M. C. Hodgson, C. E. F. Rickard, A. G. Oliver, L. Chaker, P. J. Brothers, R. D. Bolskar, F. S. Tham and C. A. Reed, Selective Supramolecular Porphyrin/Fullerene Interactions, *J. Am. Chem. Soc.*, 1999, **121**, 10487–10495.
- 23 T. Ohmura, A. Usuki, Y. Mukae, H. Motegi, S. Kajiya, M. Yamamoto, S. Senda, T. Matsumoto and K. Tatsumi, Supramolecular Porphyrin-Based Metal–Organic Frameworks with Fullerenes: Crystal Structures and Preferential Intercalation of C₇₀, *Chem. – Asian J.*, 2016, **11**, 700–704.



- 24 H. Nobukuni, T. Kamimura, H. Uno, Y. Shimazaki, Y. Naruta and F. Tani, Supramolecular Structures of Inclusion Complexes of C₇₀ and Cyclic Porphyrin Dimers, *Bull. Chem. Soc. Jpn.*, 2011, **84**, 1321–1328.
- 25 Y.-L. Cheng, L. Wei, S.-Z. Liu, X.-G. Yi, W.-T. Chen and W.-S. Lin, A novel supramolecular porphyrin-fullerene compound: Crystal structure and photophysical properties, *J. Solid State Chem.*, 2022, **311**, 123120.
- 26 T. Wakahara, K. Nagaoka, A. Nakagawa, C. Hirata, Y. Matsushita, K. Miyazawa, O. Ito, Y. Wada, M. Takagi, T. Ishimoto, M. Tachikawa and K. Tsukagoshi, One-Dimensional Fullerene/Porphyrin Cocrystals: Near-Infrared Light Sensing through Component Interactions, *ACS Appl. Mater. Interfaces*, 2020, **12**, 2878–2883.
- 27 T. Ishii, R. Kanehama, N. Aizawa, M. Yamashita, H. Matsuzaka, K. Sugiura, H. Miyasaka, T. Kodama, K. Kikuchi, I. Ikemoto, H. Tanaka, K. Marumoto and S.-I. Kuroda, Fullerene C₆₀ exhibiting a strong intermolecular interaction in a cocrystallite with C₄ symmetrical cobalt tetrakis(di-tert-butylphenyl)porphyrin, *J. Chem. Soc., Dalton Trans.*, 2001, 2975–2980.
- 28 L. H. Tong, J.-L. Wietor, W. Clegg, P. R. Raithby, S. I. Pascu and J. K. M. Sanders, Supramolecular Assemblies of Tripodal Porphyrin Hosts and C₆₀, *Chem. – Eur. J.*, 2008, **14**, 3035–3044.
- 29 D. V. Konarev, A. L. Litvinov, I. S. Neretin, N. V. Drichko, Y. L. Slovokhotov, R. N. Lyubovskaya, J. A. K. Howard and D. S. Yufit, Formation of Coordination Porphyrin Pentamers in New Supramolecular Complex of Fullerene: {(ZnTPP)₄·4-TPyP}·(C₆₀)₂·(C₆H₅CN)_{3.5}, *Cryst. Growth Des.*, 2004, **4**, 643–646.
- 30 M. Roy, I. D. Diaz Morillo, X. B. Carroll, M. M. Olmstead and A. L. Balch, Solvent and Solvate Effects on the Cocrystallization of C₆₀ with CoII(OEP) or ZnII(OEP) (OEP = Octaethylporphyrin), *Cryst. Growth Des.*, 2020, **20**, 5596–5609.
- 31 Y. Wang, H. Wu, W. Zhu, X. Zhang, Z. Liu, Y. Wu, C. Feng, Y. Dang, H. Dong, H. Fu and W. Hu, Cocrystal Engineering: Toward Solution-Processed Near-Infrared 2D Organic Cocrystals for Broadband Photodetection, *Angew. Chem., Int. Ed.*, 2021, **60**, 6344–6350.
- 32 D. V. Konarev, A. Yu. Kovalevsky, X. Li, I. S. Neretin, A. L. Litvinov, N. V. Drichko, Y. L. Slovokhotov, P. Coppens and R. N. Lyubovskaya, Synthesis and Structure of Multicomponent Crystals of Fullerenes and Metal Tetraarylporphyrins, *Inorg. Chem.*, 2002, **41**, 3638–3646.
- 33 M. M. Olmstead and D. J. Nurco, Fluorinated Tetraphenylporphyrins as Cocrystallizing Agents for C₆₀ and C₇₀, *Cryst. Growth Des.*, 2006, **6**, 109–113.
- 34 L. M. Baldauf, K. B. Ghiassi, M. M. Olmstead and A. L. Balch, Fullerene nanostructures: how the oblong shape of C₇₀ forms a cocrystal with an enormous asymmetric unit and related cocrystals, *Nanoscale*, 2020, **12**, 20356–20363.
- 35 T. Wakahara, K. Nagaoka, C. Hirata, K. Miyazawa, K. Fujii, Y. Matsushita, O. Ito, M. Takagi, T. Shimazaki, M. Tachikawa, Y. Wada, S. Yagyu, Y. Liu, Y. Nakajima and K. Tsukagoshi, Fullerene C₇₀/porphyrin hybrid nanoarchitectures: single-cocrystal nanoribbons with ambipolar charge transport properties, *RSC Adv.*, 2022, **12**, 19548–19553.
- 36 E. C. Escudero-Adán, A. Bauzá, L. P. Hernández-Eguía, F. Würthner, P. Ballester and A. Frontera, Solid-state inclusion of C₆₀ and C₇₀ in a co-polymer induced by metal-ligand coordination of a Zn-porphyrin cage with a bis-pyridyl perylene derivative, *CrystEngComm*, 2017, **19**, 4911–4919.
- 37 X. Yu, B. Wang, Y. Kim, J. Park, S. Ghosh, B. Dhara, R. D. Mukhopadhyay, J. Koo, I. Kim, S. Kim, I.-C. Hwang, S. Seki, D. M. Guldi, M.-H. Baik and K. Kim, Supramolecular Fullerene Tetramers Concocted with Porphyrin Boxes Enable Efficient Charge Separation and Delocalization, *J. Am. Chem. Soc.*, 2020, **142**, 12596–12601.
- 38 K. Chida, T. Yoshii, M. Ohwada, Y. Hayasaka, J. Komeda, R. Sakamoto, J. Maruyama, K. Kamiya, M. Inoue, F. Tani and H. Nishihara, Synthesis and electrocatalysis of ordered carbonaceous frameworks from Ni porphyrin with four ethynyl groups, *Catal. Today*, 2023, **411–412**, 113830.
- 39 T. Yoshii, G. Nishikawa, V. K. Prasad, S. Shimizu, R. Kawaguchi, R. Tang, K. Chida, N. Sato, R. Sakamoto, K. Takatani, D. Moreno-Rodríguez, P. Škorňa, E. Scholtzová, R. K. Szilagyí and H. Nishihara, Quantitative and qualitative analysis of nitrogen species in carbon at the ppm level, *Chem*, 2024, **10**, 2450–2463.
- 40 N. Sato, R. Toyoda, T. Sato, Z. L. Goo, S. Takaishi, K. Chida, T. Yoshii, H. Nishihara, K. Sugimoto and R. Sakamoto, Porphyrin/Fullerene Porous Molecular Cocrystal Featuring a Robust One-Dimensional Channel, *Precis. Chem.*, 2024, **2**, 480–487.
- 41 X. Yang, M. B. Al-Handawi, L. Li, P. Naumov and H. Zhang, Hybrid and composite materials of organic crystals, *Chem. Sci.*, 2024, **15**, 2684–2696.
- 42 N. Fukui, T. Kim, D. Kim and A. Osuka, Porphyrin Arch-Tapes: Synthesis, Contorted Structures, and Full Conjugation, *J. Am. Chem. Soc.*, 2017, **139**, 9075–9088.
- 43 J. Kim, C. Park and H. C. Choi, Selective Growth of a C₇₀ Crystal in a Mixed Solvent System: From Cube to Tube, *Chem. Mater.*, 2015, **27**, 2408–2413.
- 44 G. B. M. Vaughan, P. A. Heiey, D. E. Luzzi, D. A. Ricketts-Foot, A. R. McGhie, J. E. Fischer, Y.-W. Hui, A. L. Smith, D. E. Cox, W. J. Romanow, B. H. Allen, N. Coustel, J. P. McCauley and A. B. Smith, Orientational Disorder in Solvent-Free Solid C₇₀, *Science*, 1991, **254**, 1350–1353.
- 45 Y. Sun, X. Wang, B. Yang, M. Chen, Z. Guo, Y. Wang, J. Li, M. Xu, Y. Zhang, H. Sun, J. Dang, J. Fan, J. Li and J. Wei, Trichalcogenasupersumanenes and its concave-convex supramolecular assembly with fullerenes, *Nat. Commun.*, 2023, **14**, 3446.
- 46 Y. Wang, N. Rinn, K. Eberheim, F. Ziese, J. Christmann, A. Jana, S. Nier, N. W. Rosemann, S. Sanna and S. Dehnen, The π-trap approach for obtaining crystal structure data of inherently amorphous cluster compounds, *Nat. Commun.*, 2025, **16**, 7903.



- 47 T. D. Kühne, M. Iannuzzi, M. Del Ben, V. V. Rybkin, P. Seewald, F. Stein, T. Laino, R. Z. Khaliullin, O. Schütt, F. Schiffmann, D. Golze, J. Wilhelm, S. Chulkov, M. H. Bani-Hashemian, V. Weber, U. Borštnik, M. Taillefumier, A. S. Jakobovits, A. Lazzaro, H. Pabst, T. Müller, R. Schade, M. Guidon, S. Andermatt, N. Holmberg, G. K. Schenter, A. Hehn, A. Bussy, F. Belleflamme, G. Tabacchi, A. Glöß, M. Lass, I. Bethune, C. J. Mundy, C. Plessl, M. Watkins, J. VandeVondele, M. Krack and J. Hutter, CP2K: An electronic structure and molecular dynamics software package - Quickstep: Efficient and accurate electronic structure calculations, *J. Chem. Phys.*, 2020, **152**, 194103.
- 48 Y. Xu, S. Zhang, W. Wu and P. Su, Assessments of DFT-based energy decomposition analysis methods for intermolecular interactions, *J. Chem. Phys.*, 2023, **158**, 124116.
- 49 S. Grimme, Supramolecular Binding Thermodynamics by Dispersion-Corrected Density Functional Theory, *Chem. - Eur. J.*, 2012, **18**, 9955–9964.
- 50 M.-S. Liao, J. D. Watts and M.-J. Huang, Dispersion-corrected DFT calculations on C60-porphyrin complexes, *Phys. Chem. Chem. Phys.*, 2009, **11**, 4365–4374.
- 51 K. W. Chapman, G. J. Halder and P. J. Chupas, Pressure-Induced Amorphization and Porosity Modification in a Metal–Organic Framework, *J. Am. Chem. Soc.*, 2009, **131**, 17546–17547.
- 52 B. Yeskendir, J.-P. Dacquin, Y. Lorgouilloux, C. Courtois, S. Royer and J. Dhainaut, From metal–organic framework powders to shaped solids: recent developments and challenges, *Mater. Adv.*, 2021, **2**, 7139–7186.
- 53 A. Liang, J. Gonzalez-Platas, R. Turnbull, C. Popescu, I. Fernandez-Guillen, R. Abargues, P. P. Boix, L.-T. Shi and D. Errandonea, Reassigning the Pressure-Induced Phase Transitions of Methylammonium Lead Bromide Perovskite, *J. Am. Chem. Soc.*, 2022, **144**, 20099–20108.
- 54 (a) N. Sato, CSD communication, 2026, CCDC 2527177: Experimental Crystal Structure Determination, 2026, DOI: [10.5517/ccdc.csd.cc2qtqv4](https://doi.org/10.5517/ccdc.csd.cc2qtqv4); (b) N. Sato, CSD communication, 2026, CCDC 2527178: Experimental Crystal Structure Determination, 2026, DOI: [10.5517/ccdc.csd.cc2qtqw5](https://doi.org/10.5517/ccdc.csd.cc2qtqw5); (c) N. Sato, CSD communication, 2026, CCDC 2527179: Experimental Crystal Structure Determination, 2026, DOI: [10.5517/ccdc.csd.cc2qtqx6](https://doi.org/10.5517/ccdc.csd.cc2qtqx6).

